

Investigation of Wear Behavior of TiC Additive Stainless Steel Coatings Produced by High Pressure Cold Spray Method

Olcay Kaya¹, Salih Gül¹, Ediz Ercenk^{1,2*}

¹ Sakarya University, Faculty of Engineering, Metallurgical and Materials Engineering Department, Esentepe Campus, Sakarya, Türkiye, olcay.kaya4@ogr.sakarya.edu.tr, salih.gul@ogr.sakarya.edu.tr, ror.org/04ttnw109

² Sakarya University, Natural Resources and Waste Assessment Laboratory (DOKADEM), Esentepe Campus, Sakarya, Türkiye, ercenk@sakarya.edu.tr, ror.org/04ttnw109

*Corresponding Author

ARTICLE INFO

ABSTRACT

Keywords:
Cold Spray
Stainless steel
TiC
Wear resistance
Hardness

Article History:

Received: 21.08.2025

Revised: 27.09.2025

Accepted: 01.10.2025

Online Available: 12.12.2025

In this study, commercial 430L stainless steel powder and TiC powder were mixed in specific proportions. The prepared powders were coated onto steel substrates using the high-pressure cold spray method (HPCS). Micro-hardness and surface roughness measurements were performed after coating. The resulting materials were examined using an optical microscope and a scanning electron microscope (SEM) for microstructural analysis. X-ray diffraction analysis (XRD) was used for phase analysis. Furthermore, the coatings were abraded to the ball-on-disc wear level, and wear scars were analyzed using SEM and energy dispersive X-ray Spectroscopy (EDS) to investigate wear mechanisms. The results indicate that TiC addition increases hardness and wear resistance. The wear rates were obtained in the range of 1.24-1.57 mm³/Nm with increasing TiC addition. Changes in wear mechanisms were also detected with increasing TiC addition. Furthermore, the hardness values were obtained in the range of 256-391 HV depending on the TiC addition.

1. Introduction

Cold spray (CS) is an innovative coating technology based on solid-state deposition that has attracted attention in surface engineering in recent years. This method accelerates particles to supersonic speeds by a carrier gas (usually nitrogen or helium) and collides with the substrate surface. Due to the high kinetic energy, the particles undergo plastic deformation and bond to the surface during the impact. Because this bonding occurs entirely in the solid state, the melting-related problems common in thermal spray methods are avoided [1].

The CS method is essentially based on generating a high-pressure gas stream through a nozzle. The gas passing through this nozzle accelerates the powder particles to speeds between 300 and 1500 m/s, forcing them to impact the surface [2]. The particle speeds reached at these speeds cause

plastic deformation on the surface during impact, creating the necessary conditions for bonding. Typically, particles with a 5–100 µm diameter are used, and the processing temperature is well below the particle's melting point. This largely preserves structural, microstructural integrity, and chemical composition [3]. The particle impact process for cold-sprayed powders (from initial contact to the complete dissipation of kinetic energy) takes approximately 100 ns. [4] In the cold spray method, particles are sprayed onto the substrate at supersonic speeds (300–1200 m s⁻¹) [5]. Since the contact time of the spray particles with the hot gas is relatively short and the gas cools rapidly as it expands in the divergent section of the nozzle, the temperature of the particles remains significantly below the initial gas preheating temperature. Therefore, deposition can be easily controlled to occur below the melting temperature of the raw material powder, producing deposits from solid-

state particles. Thus, Cold Spray deposits are essentially free of thermally induced defects commonly observed in conventional thermal spray deposits, such as oxidation, evaporation, gas release, shrinkage porosity, and thermally induced residual stresses [6]. Using cold spray techniques, it is also possible to achieve extremely dense and heavy coatings with thicknesses ranging from 100 μm to 1500 μm [4, 7]. In cold spray, the carrier gas is heated not to melt the powder, as in other thermal spray methods, but to increase its velocity. The carrier gas passing through the nozzle expands, converting enthalpy into kinetic energy. Therefore, the carrier gas cools rapidly and leaves the nozzle at lower temperatures [8].

Pure metals such as Ni, Al, and Zn, as well as their composites, are common ductile materials successfully sprayed onto various substrates using the Cold Spray (CS) method. Furthermore, coating and substrate adhesion are significantly affected by the substrate hardness. Due to its low plastic deformation properties, CS is difficult to deposit on ceramics and hard carbides. In cold spraying, plastic deformation can be increased by increasing the sprayed particle velocity for more efficient deposition. However, for materials with low ductility, such as ceramics, increasing the particle velocity significantly increases the likelihood of fracture. Therefore, the cold spray method allows the deposition of ceramic materials with metal binders. In the deposition of ceramic/metal materials, the soft metal component acts as a binder and facilitates bonding. However, obtaining cermet coating layers with high carbide content remains challenging. The amount of binder and ceramic is critical for achieving successful deposition layers. Although the increase in particle speed in the CS process increases the plastic deformation of the metal (binder) phase, it causes the ceramic particles to break and disintegrate, making deposition difficult [8]. Recently, studies on the coating of ceramic/metal based powders using the cold spray method have become popular. In particular, the mechanical properties of cermet coatings, such as wear, were investigated. Jagadeeswar et al. reported the wear and corrosion behavior of Ni-WC cermet based coatings produced using cold spray [9]. Adebisi et al. characterized the coatings they produced by

adding SiC to the Ti-6Al-4V alloy [10]. In another study, the wear behavior of WC-17Co coatings was studied [11]. In these similar studies, the mechanical properties of cermet coatings formed with hard ceramic particle reinforcement and relatively soft metal matrix were investigated and the effects of ceramic additives were investigated.

In this study, powders produced by mixing 430 series stainless steel powder with TiC powder were coated onto plain carbon steel substrates using the cold spray method. 430 series stainless steels have high corrosion resistance but low mechanical strength. The average mechanical properties of 430 stainless steels are; hardness value: 160-200 HV, comprehensive strength: 200-350 MPa. They are suitable coating materials for cold spray, but the resulting coatings will have low mechanical strength. TiC, on the other hand, has very high mechanical, the hardness values of TiC are around 2800-3200 HV and the compressive strength values are around 3000-4000 MPa. and thermal stability, but such rigid and stable powders are not suitable for cold spray coating alone. This study aimed to produce metallic matrix and ceramic-reinforced composite coatings and investigate their wear properties by utilizing the favorable coating properties of stainless steel and the mechanical resistance of TiC powders.

2. General Methods

In this study, 430L stainless steel powder and 430L stainless steel powders with Titanium Carbide (TiC) additives at rates of 10%, 20% and 30% by weight were coated on the surface of steel substrate (CK45) by high-pressure cold spray (HPCS) method. 430L stainless steel powder (Fe: Bal., C:<0.03, Si:0.9, Cr:17, Mn:0.1) and Höganäs x-TiC series TiC powder (Ti:79.4, C:19.6, O:1) were used in the coating processes. CK45 steel substrates were subjected to a sandblasting process to remove oxide and dirt layers on the surface. This process was carried out to increase the surface roughness and facilitate the mechanical bonding of the cold spray coating. TiC added powder mixtures were prepared at 10%, 20% and 30% by weight. The mixture was mixed for 1 hour in a low-speed mechanical mixer to obtain a homogeneous

mixture. SEM images of the coating powders are shown in Figure 1. The images show the spherical structure of the stainless steel powders, while the angular, irregular structure of the TiC powder is observed. The stainless steel and TiC powder sizes are similar, ranging from approximately 20 to 60 μm . Nitrogen was used as the carrier gas in the HPCS system, and the system was operated with a gas pressure in the range of 2–5 MPa. The powder particles exiting the nozzle reached 1000–1500 m/s speeds and impacted the CK45 substrate. As a result of this high-speed impact, the particles underwent plastic deformation and were mechanically bonded to the substrate surface. The samples prepared after coating were cut using a Mecatome T265 sample cutting machine, and, by standard metallography procedures, they were sanded with 200, 400, 800, and 1000 grid SiC-based sandpapers and polished with alumina paste. After metallography, microstructural examinations of the coatings were performed under an optical microscope.

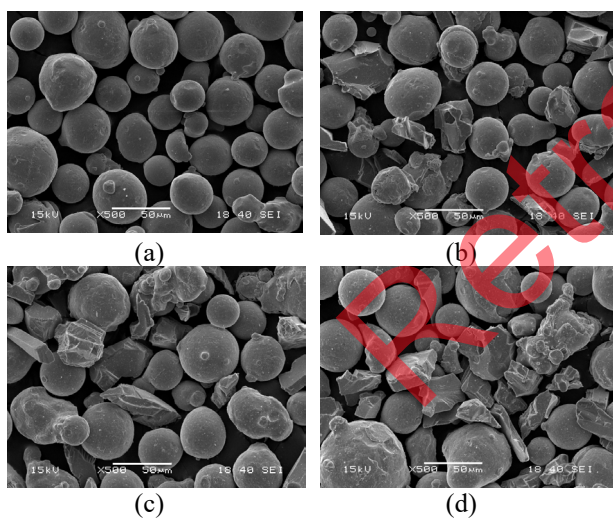


Figure 1. SEM images of coating powders (a) 430L powder (b) 430L powder coating with 10 wt.% TiC (c) 430L powder coating with 20 wt.% TiC (d) 430L powder with 30 wt.% TiC

Wear tests were carried out by creating planar indentations using a 10 mm diameter alumina ball. Wear tests were applied with a load of 5 N, a distance of 250 meters, and a speed of 10 m/s. Wear tests were carried out with a CSM brand device in a ball-on-disc system according to ASTM G133 standards. Scanning electron microscope and EDS analysis were used to examine the coating structures and characterize the wear scars after abrasion (JEOL-6060). X-ray

diffraction analysis (XRD-RIGAKU D MAX-2200) was applied for phase analysis after coating. 2 Theta angle was 10° – 90° and $\text{CuK}\alpha$ was 1.54056 in the XRD analysis. Microhardness measurements were carried out using a Leica VMHT hardness device with a Vickers test tip. Hardness tests were carried out with a 200 g load for 15 seconds. The tests were repeated five times, and the average was taken. Surface roughness measurements were also performed after coating. Load selection for hardness measurements was carried out experimentally. The load providing the optimum hardness signature was selected.

3. Results and Discussion

Figure 2 shows optical section images of coatings containing 10 and 30 wt% TiC. Coating thicknesses ranged from 200 to 350 μm . No significant effect of TiC addition on coating thickness was detected. Optical microscope images are shown in Figure 3. In the 30% TiC-doped sample shown in Figure 3(a), it is observed that the carbide particles are clearly distributed within the matrix and concentrated in some areas. The carbides mostly have irregular geometries, and local agglomerations occur where they are not homogeneously distributed. However, structural continuity is maintained along the coating-substrate interface. The 20 wt.% TiC-doped sample in Figure 3(b) was examined similarly without etching, and it was observed that a significant portion of the pore-like voids contained carbides. These carbide formations are visible in the areas marked with red circles. The presence of carbides indicates that the matrix has been strengthened regarding hardness and wear resistance. The 10 wt.% TiC-doped sample is presented in Figure 3(c). The carbides are more limited and dispersed in this sample, and the structure generally appears more homogeneous. The porosity rate is lower than in the other doped samples.

The measured hardness values and surface roughness values are given in Figure 4. As a result of the Vickers microhardness measurements, the average values were 256 HV for the unalloyed 430L stainless steel coating, 309 HV for the 10% TiC-added sample, 369 HV for the 20% TiC-added sample, and 391 HV for

the 30% TiC-added sample. In the literature, hardness values of 120-240 HV have been measured for Al-9% Sn-3% Zn + Al₂O₃-based cermet coatings applied using the cold spray method. Hardness values of 440 HV were achieved for h-BN7.5+7 wt% Cr₂O₃ based cermet coatings. The hardness values obtained in this study are also close to these results [12].

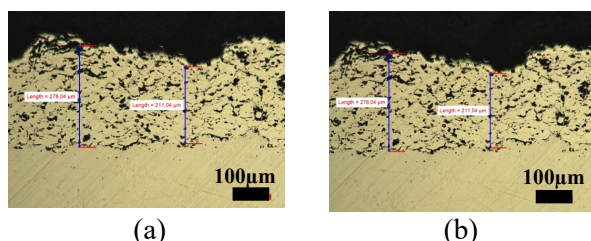


Figure 2. The optical images taken from the cross-section a) 10 wt.% TiC doped coating b) 30 wt.% TiC doped coating

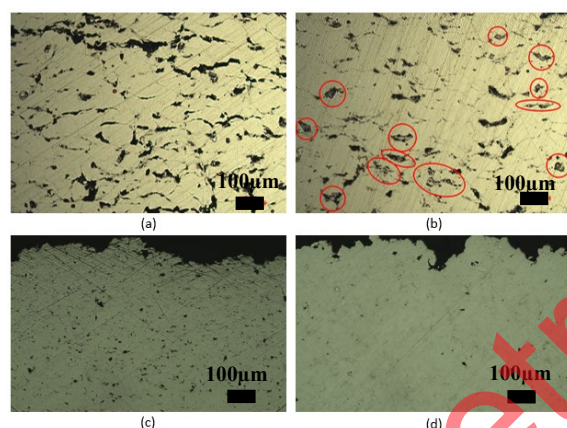


Figure 3. Optical microstructure images (a) 430L powder coating with 30 wt.% TiC (b) 430L powder coating with 20 wt.% TiC (c) 430L powder coating with 10 wt.% TiC (d) 430L powder coating

The average surface roughness values were 4.91 μm for the 430L stainless steel coating, 7.85 μm for the 10 wt.% TiC-added sample, 11.05 μm for the 20 wt.% TiC-added sample, and 14.62 μm for the 30 wt.% TiC-added sample. The hardness and surface roughness values appear to increase with increasing TiC addition. The hardness of the TiC powder is very high compared to the 430 series stainless steel. TiC particles are thought to significantly increase coating hardness by acting as a composite. The increase in surface roughness due to TiC addition is thought to be related to the mechanical effects (impact, embedding) created by the hard TiC particles on the surface during coating and the resulting voids/cavities resulting from the inability of

some TiC particles to adhere to the surface during coating.

Hardness is the resistance a material exhibits to indentation. When hard particles are embedded in a soft matrix, the average hardness of the material increases. The composite effect limits plastic deformation in the soft matrix, thus reducing the resulting hardness marks. It is observed that the agglomeration effect (for TiC particles) in surface roughness, the mechanical deformation effect created by hard TiC particles in soft stainless steel, and the porosity effects created by TiC particles that cannot be mechanically bonded to the surface significantly increase the total surface roughness, and the roughness values increase considerably with increasing TiC addition.

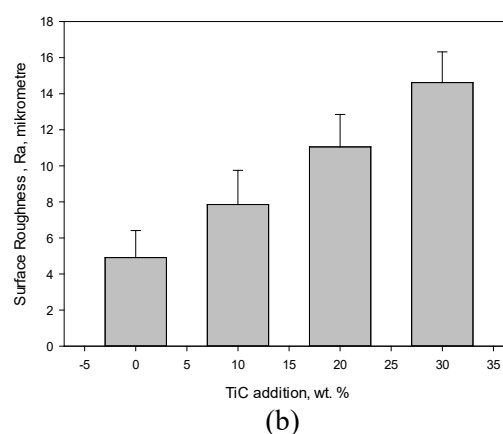
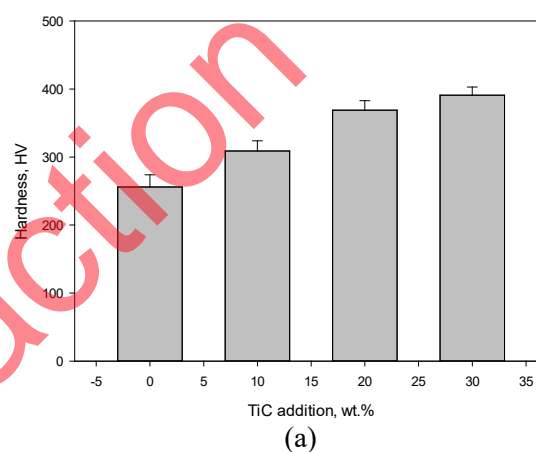


Figure 4. Hardness and surface roughness results for the coatings a) Hardness b) Surface roughness

The frontal SEM image of coatings produced using undoped 430L stainless steel powder is shown in Figure 5. The chemical composition of the 430L stainless steel powder was determined to be 64.14% iron (Fe) and 10.70% chromium (Cr), as well as containing specific amounts of oxygen (22.76%), silicon (1.28%), aluminum

(0.34%), phosphorus (0.23%), and trace amounts of nickel (0.55%). The coating is observed to be homogeneous and slightly rough in certain areas, while irregular and rough in others. EDS analysis of the coating shows the chemical composition characteristic of stainless steel, and the oxygen content is high due to oxidation on the surface. This indicates that some oxidation occurred during the coating. In the regional EDS analysis of the overall SEM image (Figure 6), the Fe, Al, Cr, and Si contained in the stainless steel content are the strongest peaks, consistent with the chemical composition.

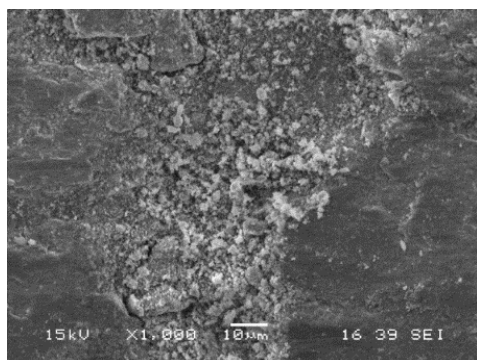
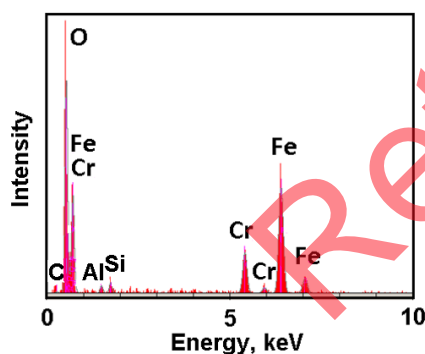


Figure 5. SEM image of the coating made with 430L powder



Elt	Intensity(c/s)	Conc
C	1.40	0.583
O	163.12	30.348
Al	6.97	1.031
Si	9.80	1.269
Cr	52.86	11.235
Fe	148.34	55.534

Figure 6. EDS analysis of coating made with 430L powder

Figure 7 shows an SEM image taken from a 10% TiC-additive coating. The SEM-EDS analysis performed on the 10 wt.% TiC-additive coating is presented as EDS maps to visualize the TiC grains. The SEM image shows that TiC grains are embedded in the stainless steel matrix. The intense carbon signal obtained from the TiC grain region confirms the presence of TiC particles in

this region. Considering that the TiC powders used have a size range of 15-45 µm, the TiC-dense region detected in the image is over 100 µm in size. This indicates that the TiC powders partially agglomerated during coating. The risk of agglomeration is a common problem in powder metallurgy, and the risk increases as the powder size decreases. Powders with small powder sizes and high surface areas have high surface energy and tend to agglomerate, thus reducing their surface energy.

Furthermore, the static charge of the powders promotes their adhesion. The temperature effect during coating may also have influenced the tendency to agglomerate. Considering all these parameters, the TiC powders are somewhat agglomerated and embedded in the stainless steel matrix. On the other hand, the strong carbon signals obtained from the EDS analysis indicate that the TiC powders are not degraded during the coating process. TiC powders are known to be thermally resistant. The risk of oxidation generally begins at temperatures above 700°C. Although the temperatures reached during coating are around this temperature, it is thought that the TiC powders remain broadly stable, and the strong carbon signals in the EDS analysis support this idea. Cr appears to be homogeneously distributed in the region outside the TiC particles. The macro SEM image taken at lower magnification (Figure 8) shows regions rich in TiC particles distributed throughout the coating. The different sizes of these regions indicate that TiC-based grains of various sizes, formed by the agglomeration of the TiC particles, are embedded in the stainless steel matrix. Agglomerated TiC particles were embedded and dispersed in the stainless steel matrix in clumps of different sizes, causing the formation of TiC islands of different sizes.

Figure 9 shows the SEM image and EDS map of a sample containing 20 wt. % TiC. The SEM image of higher magnification clearly shows the TiC particle within the stainless steel matrix. In the EDS analysis, the O signals decreased in the region where the Ti and C signals were high, indicating that the TiC particle remained stable. Furthermore, when the image scale is examined, it is seen that the TiC region is around 15-30 µm. The TiC powders used are in this size range.

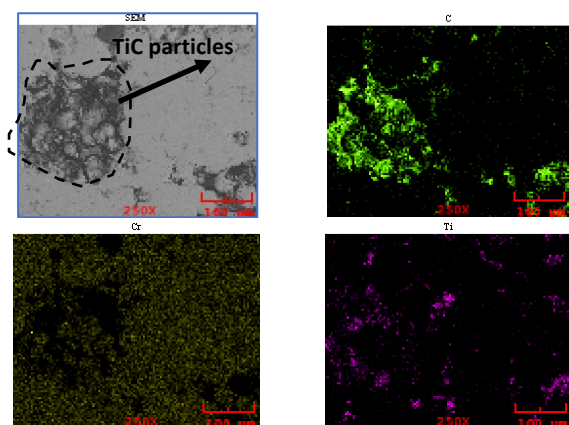


Figure 7. SEM image and EDS maps of the coating made with 10 wt.% TiC added 430L powder

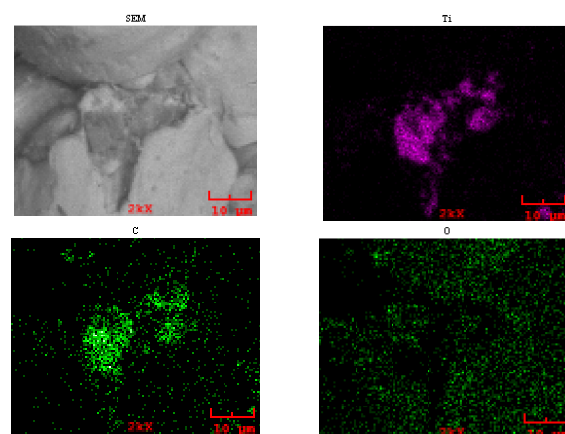


Figure 9. SEM image and EDS maps of the coating made with 20 wt.% TiC added 430L powder

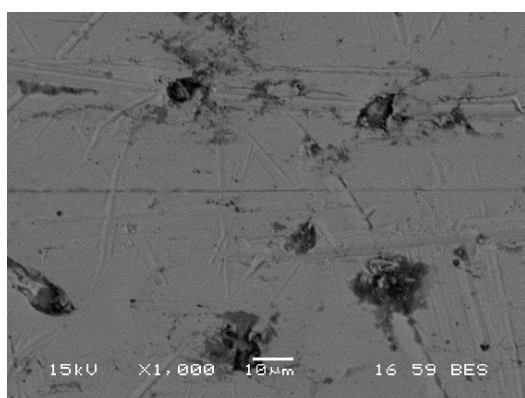


Figure 8. SEM image of the coating made with 10 wt.% TiC added 430L powder

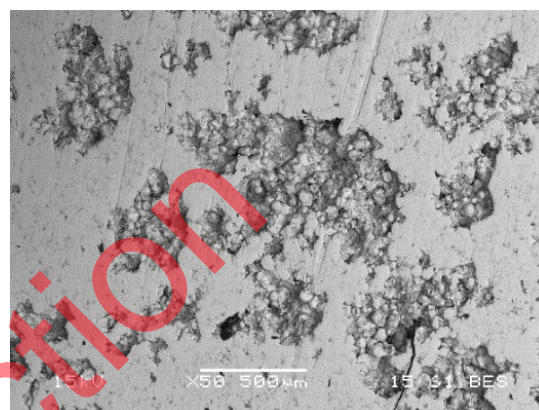


Figure 10. SEM image of the coating made with 430L powder with 20 wt.% TiC additive

It was observed that the TiC powders were not completely agglomerated, and some powders remained in the stainless steel matrix without agglomeration. Figure 10 shows TiC-based agglomerates of various sizes formed due to the agglomeration of TiC particles in the lower magnification macro image taken from the same sample. This indicates that the tendency for agglomeration increases with the increase in the TiC content, and that TiC-based regions of various sizes form on the coating surface.

Figure 11 shows the SEM image and EDS map from a 30% TiC-doped coating. The image is similar to other doped coating samples, and the TiC particles are observed embedded within the stainless steel matrix. The absence of Fe and Cr signals from the relevant area confirms that the area is TiC-based.

Figure 12 shows an SEM image from the same TiC-based area at a higher magnification. A striking result is the presence of voids in the image. These voids, also observed in the optical images of the coatings, are thought to be caused by TiC particles that cannot adhere to the surface and lose their positions. TiC particles that fail to comply with the surface during coating cause void formation.

Figure 13 shows the XRD analysis results taken from the coatings. XRD analyses of the coatings revealed Khamrabaevite (TiC-01-089-3828), Fe-Cr-based stainless steel phase (00-034-0396), TiO (01-086-2352), and magnetite (Fe₃O₄-01-072-2303) phases. The stainless steel phase was common to all coatings, and no marginal difference in peak intensities was observed. The intense peaks of the TiC phase overlap with the other phases and have an independent peak at approximately 72.5°. This peak intensifies with increasing TiC content in the coating. A similar pattern is observed for the peak at 41.8°, where the most intense peak of the TiC phase is located.

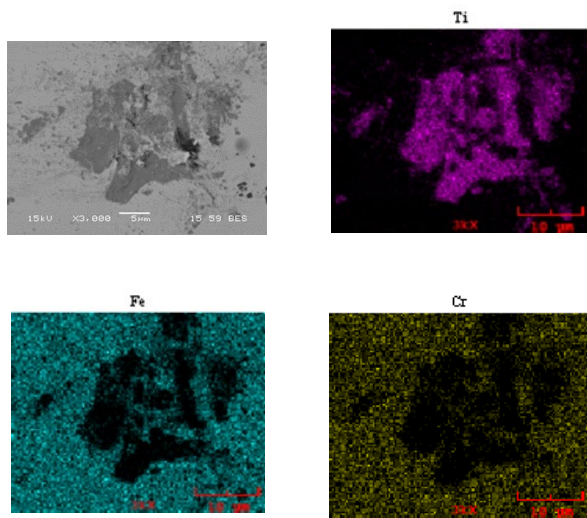


Figure 11. SEM image and EDS maps of the coating made with 30 wt.% TiC added 430L powder

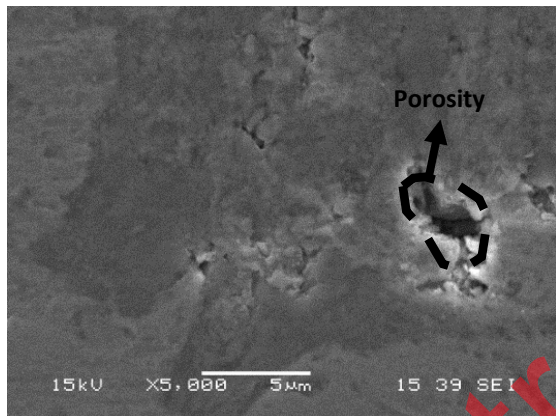


Figure 12. SEM image of the coating made with 430L powder with 30 wt.% TiC additive

Magnetite and TiO phases are thought to form by partial oxidation of the coating. Fe within the stainless steel and Ti within the additives oxidized to some extent to form these phases. These phases exhibit intense peaks around 35°C. This peak was observed to increase in the 10% TiC-added sample and decrease in the 20% and 30% TiC-added samples. The weakness of this peak in the unadded coating supports the idea that oxidation occurs within the TiC rather than within the Fe in the stainless steel. At 20% and 30% TiC additions, the oxidation effect is thought to be related to the agglomeration effect that increases with increasing TiC content in the coating. The decreased contact area due to agglomeration is thought to slow down oxidation.

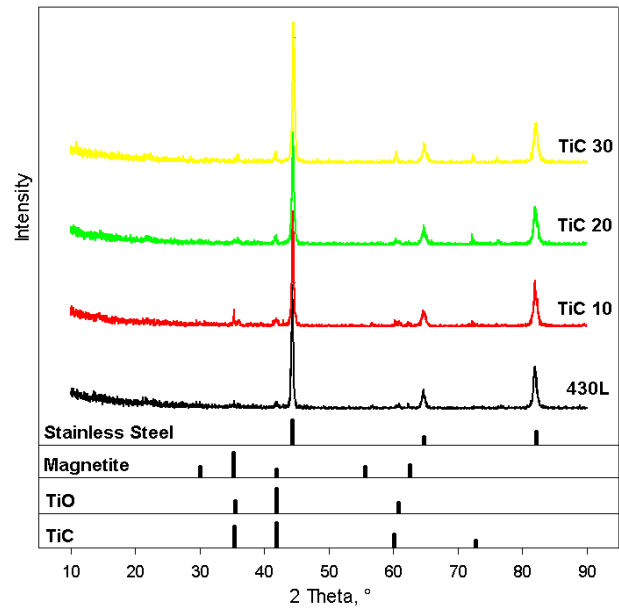


Figure 13. XRD analysis of the coatings

Figure 14 shows the wear test results. Wear rates were determined to be $1.24-1.57 \times 10^{-5} \text{ mm}^3/\text{nm}$, depending on the TiC content. The results show that wear rates decrease with increasing TiC content in the coating. The study's primary objective was to produce a metal-matrix ceramic particle-reinforced composite coating and to improve the wear resistance of the stainless steel coating. The results show that TiC reinforcement increases wear resistance. In composite materials, the reinforcement element is generally harder and high mechanical resistance, increasing wear resistance. 430 series stainless steels, a ferritic stainless steel, are not resistant to wear, with an average hardness of 160-200 HV. TiC, on the other hand, has high mechanical/thermal resistance among advanced ceramic materials, with hardness values around 2800-3200 HV. As can be seen, the hardness of the ceramic particles appears to be more than ten times that of the stainless steel matrix. Thus, TiC particles significantly increased the wear resistance of the 430L stainless steel-based coating. Ehvazi et al. reported in their studies on the wear of cold spray based coatings produced by adding SiC particles to Al powder that the SiC addition increased the wear resistance of the pure Al coating [13].

Figure 15 shows the friction coefficient results obtained in the wear tests of the samples. The friction coefficient values were found to be in the range of 0.55-0.9 μ . The friction coefficients decreased with increasing TiC addition. It can be

seen that the change in the friction coefficient is affected by different parameters. First, considering oxidation, it was determined that both the stainless steel matrix and the TiC particles were partially oxidized. Oxide layers can affect the friction coefficient in different ways. Hard, brittle, and irregular oxide layers can increase the friction coefficient. Soft, thin, and non-adhesive oxide layers, on the other hand, can cause a relatively slippery film to form on the surface. Considering that more TiC powder is converted to TiO with increasing TiC addition, we can say that the oxide amount increases relatively with increasing TiC content. Consequently, if increasing oxidation with increasing TiC content causes a decrease in the friction coefficient, the resulting oxide films may act as a slippery layer.

On the other hand, heating due to friction promotes oxidation. TiO was detected in XRD analysis instead of TiO₂. This indicates that TiC does not have a very high oxidation effect, thus the heat effect is relatively low, and the heating is not excessive. The absence of a high heat effect indicates a low friction effect; that is, the resulting interlayer is slippery. This supports the fact that oxidation reduces the friction coefficient. For titanium, the +4 oxide form (TiO₂) is more stable than the +2 oxide form (TiO). A high oxidation concentration is required for the formation of TiO₂. The agglomeration effect on TiC particles is thought to reduce Ti-O contact. Thus, the TiO structure is thought to remain stable at relatively low oxygen concentrations. When evaluated in terms of temperature, TiO₂ can be formed at relatively lower temperatures (below 1000°C), while TiO remains stable at higher temperatures (above 1000°C). Therefore, TiO₂ is expected to form under the coating conditions. However, oxygen

concentration is thought to be a more effective parameter than temperature.

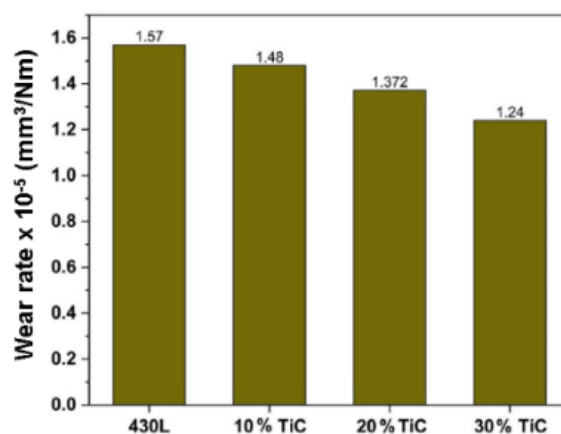


Figure 14. Wear test results of coatings according to the TiC addition

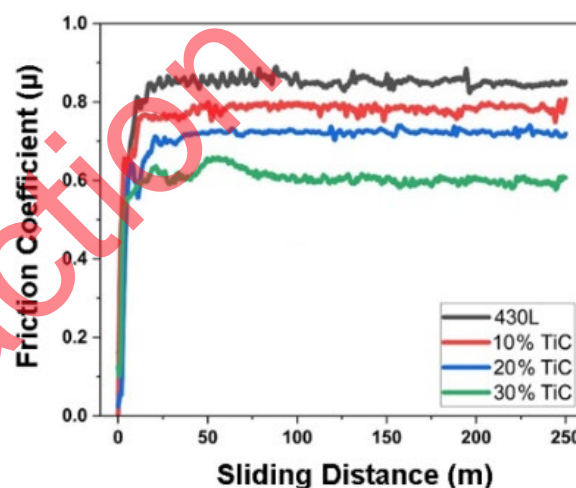


Figure 15. Friction coefficients obtained in the wear tests of the coatings

Figure 16 shows 3D profilometer images of wear samples. The images show that wear scar depths decrease with increasing TiC addition. The results support the wear rate and coefficient of friction results. While deep, continuous scars are visible in the profilometer images of samples without TiC addition and with 10 wt.% TiC addition, the 20 wt.% and 30 wt.% TiC addition samples exhibit shallower scars. Localized deep areas are noticeable within the scars in the 20 wt.% and 30 wt.% TiC addition samples. This suggests that TiC particles are breaking off during wear in these samples, forming voids in their place.

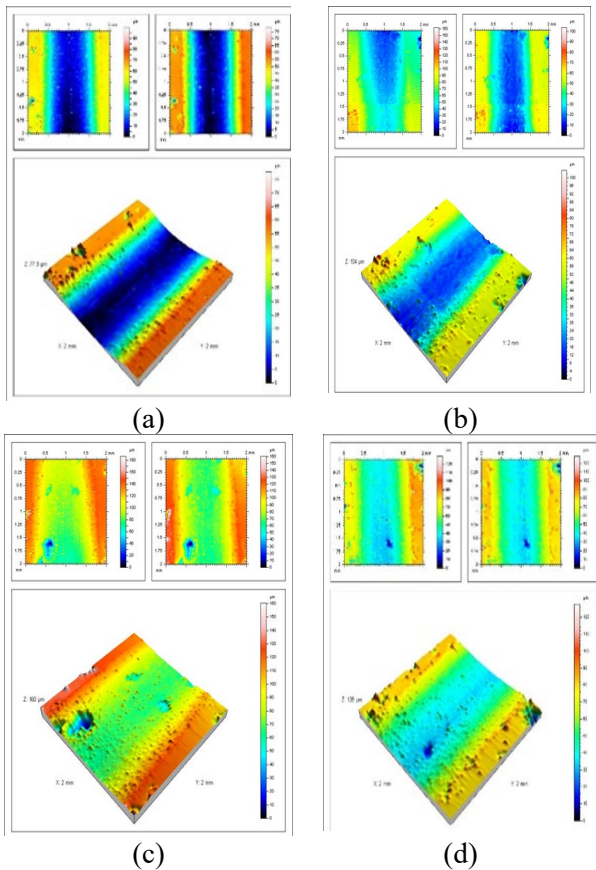


Figure 16. 3D profilometer images taken from wear tracks a) The coating without TiC b) The coating with 10 wt.% TiC c) The coating with 20 wt.% TiC d) The coating with 30 wt.% TiC

The data obtained indicate that increasing amounts of TiC additive reduce the wear rate and therefore significantly improve the wear resistance of the coating. However, the improvement rate decreases as the additive content increases, meaning the benefits are more limited after a certain additive level. It was also noted that as the TiC content rises, the coefficient of friction decreases, and the system exhibits more stable frictional behavior.

SEM images taken from the wear tracks following the wear tests are shown in Figure 17. Intense abrasive wear marks are visible in the wear tracks of the samples without TiC and with 10% TiC. The higher friction coefficients in these samples compared to the other samples indicate that abrasive wear is the primary wear mechanism in these samples. The primary causes of abrasive wear are hard particles or rough areas on the worn surfaces, as well as scraping other surfaces. In the untreated sample, the underlying cause of the abrasive effect is unlikely to be hard particles. This is because stainless steel is

relatively soft, and particle breakage is doubtful. In this sample, the rough surfaces are thought to have caused the abrasive effect. In the sample with 10 wt.% TiC, the abrasive effect can be attributed to the shearing and dislocation of TiC particles, resulting in the TiC particles becoming trapped between the surfaces during wear. In other words, a mechanism known as three-body wear may have occurred, resulting in hard abrasive wear marks due to the compression of TiC particles between two surfaces and the resulting plowing effect. This is supported by the high coefficient of friction in the 10% TiC-added sample. Wear marks on the 20 wt.% and 30 wt.% TiC-added samples indicate a decrease in abrasive grooves, indicating a shift in the wear mechanism from abrasive to adhesive. Wear marks on these samples were adhesion rather than scraping. The most critical parameter supporting adhesive wear is surface adhesion. This is frequently seen on metal surfaces with lower hardness than ceramics. On the other hand, the high surface energy on metal surfaces promotes adhesion between surfaces. In this study, alumina balls were used during abrasion. In other words, the ceramic/metal surfaces served as wear surfaces, so it may not be accurate to talk about adhesion due to surface energy. Another parameter supporting adhesive wear is surface roughness. As surface roughness increases, the risk of adhesive wear increases. Rough areas on the surface can cause adhesion by creating a microwelding effect. It is believed that surface roughness increases slightly due to the increasing TiC content in the coatings. Agglomeration of TiC particles and irregular accumulation on the surface will increase roughness. An expected result would be that the wear mechanism shifts to an adhesive mechanism with increasing surface roughness.

On the other hand, it is thought that the TiC particles dislodge during wear and create cavities/voids on the surface, which also increases surface roughness. The measured surface roughness values support this idea, and it was determined that surface roughness values increase with increasing TiC addition. These mechanisms may have caused the wear mechanism to shift from abrasive to adhesive in the 20 wt. % and 30 wt. % TiC-added samples.

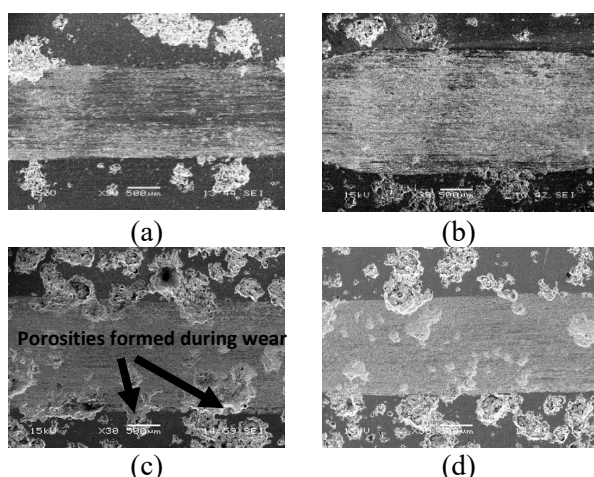


Figure 17. SEM images taken from wear tracks a) The coating without TiC additive b) The coating with 10 wt. % TiC additive c) The coating with 20 wt. % TiC additive d) The coating with 30 wt. % TiC additive

Figure 18 shows SEM images and elemental analysis values of abrasion powders obtained after abrasion. The irregularly shaped, varying sizes of the powders indicate that the powders have undergone significant deformation during coating and wear test. The stainless steel powders, which were spherical before coating process, appear to have completely lost their shape. Because the abrasion powders were to be compared with each other in terms of elemental analysis, the same amount of abrasion powder was subjected to analysis. SEM images of all abrasion powders show that irregular, variably shaped, and sized coatings were detached from the coating surface as powder particles and larger fragments. The elements Fe, Cr, and O were detected in the powders obtained from the abrasion tests of the TiC-free sample. O was detected in all the abrasion powders obtained from the abrasion tests, indicating oxidation during abrasion. The high concentration of Fe and Cr in the abrasion powders indicates that the stainless steel was removed from the surface. Small fragments remaining at the interface, as the stainless steel coating particles left the surface, may have caused abrasive wear. On the other hand, the hard alumina ball appears to have scratched the surface, causing fragments to break off. In the 10 wt.% TiC-added sample, the elements Fe, Cr, and O are again visible. This time, it was observed that some Ti was incorporated into the abrasion powders. TiC particles appear to have been dislodged during wear. It is believed that the scraping effect

increases with increasing TiC particle content. The Fe and Cr intensities obtained from the abrasion dust of this sample are higher than those obtained from the abrasion dust of the undoped sample. This supports the idea that a wear environment with strong scraping and plowing effects was formed. The abrasive grooves obtained in the wear SEM images also support this idea.

The elements Fe, Cr, O, and Ti are also prominent in the analyses of the abrasion dusts obtained from the abrasion tests of the 20 wt.% TiC-doped sample. The Ti intensity increased as the Ti content increased, indicating that more TiC was dislodged with the increasing Ti content. The Fe and Cr intensities decreased in this coating. It can be assumed that less stainless steel was removed from the coating with increasing TiC content. In fact, the abrasion dusts obtained from the 20 wt.% and 30 wt.% TiC-doped coatings were slightly less abundant than those obtained from the abrasion of other coatings. Considering that less coating is removed as the TiC content increases in the coating, the wear mechanism is likely to change. The presence of more TiC in the coating will cause more TiC particles to be displaced during wear, creating voids behind them. Under normal conditions, pits and voids formed on the surface of a material may not significantly affect surface roughness. The primary factor affecting surface roughness is the protrusions on the surface. However, with the increased TiC content in the coating, the formation of numerous pits/voids during intense wear, coupled with the wide variety of shapes and sizes of these voids, may have increased surface roughness. The increase in surface roughness may have also caused the wear mechanism to shift from abrasive to adhesive wear. In the sample containing 30% TiC, the elements Fe, Cr, O, and Ti were also detected, with the Ti content increasing compared to the other coatings, while the Fe and Cr content decreased. In this sample, wear is likely adhesive, with a smearing rather than a removal of particles. The removal rate, friction coefficient, and wear scar SEM images support this idea.

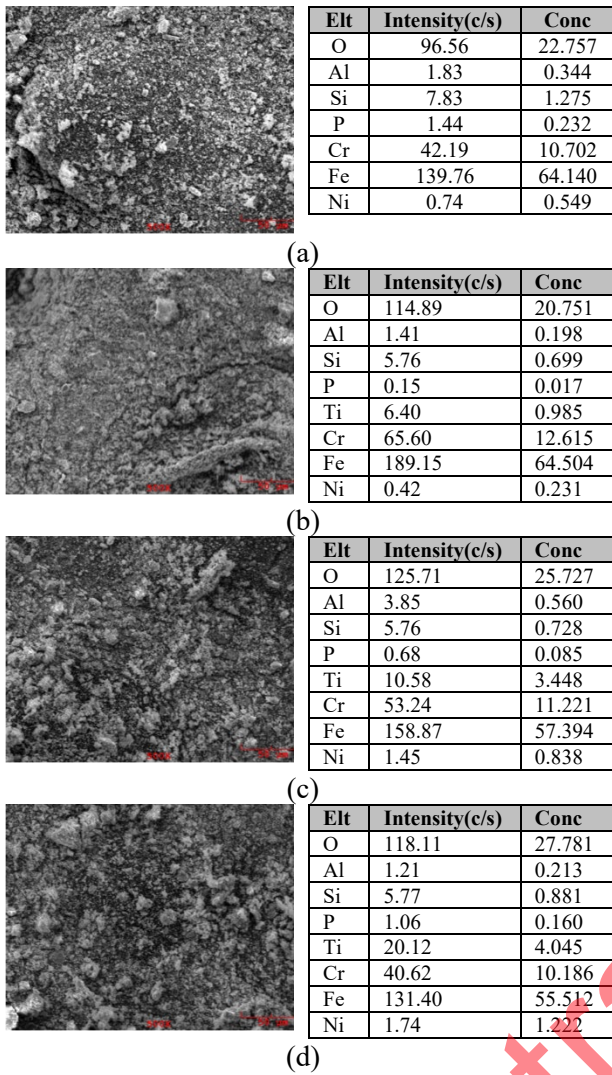


Figure 18. SEM images and EDS analyses of abrasion powders obtained after wear tests (a) The powders without TiC b) The powders with 10 wt. % TiC c) The powders with 20 wt. % TiC d) The powders with 30 wt. % TiC

4. Conclusion

This study produced composite-based coatings using the cold spray method by adding commercial TiC powder to commercial 430L stainless steel powder to increase its mechanical strength. The following results were obtained in the study;

1. The addition of TiC significantly increased the hardness and wear resistance of the stainless steel coating. Hardness values increased from 256 HV for the untreated coating to 391 HV for the 30 wt.% TiC added coating.
2. It was observed that the surface roughness of the coatings increased with increasing TiC content. It is believed that some

agglomeration of the TiC powder during coating caused the coating surface roughness to increase. Additionally, some voids were observed on the surface, indicating that some TiC particles failed to adhere to the surface during coating, creating voids. TiC additive has increased the surface roughness significantly, surface preparation (grinding) can be necessary to reduce the roughness values after coating.

3. It was determined that the TiC particles that failed to adhere to the surface and the TiC particles that agglomerated during coating caused the surface roughness. Wear mechanisms also changed with the addition of TiC. Strong abrasive wear patterns were observed in coatings without TiC and 10 wt.% TiC, while adhesive wear was dominant in 20 wt.% and 30 wt.% TiC coatings.
4. Based on the study results, the highest wear resistance was achieved with a 30 wt.% TiC added coating. However, with increasing TiC addition, an increase in TiC particles that fail to adhere to the coating surface is observed. Therefore, it is believed that adding hard powders like TiC to a stainless steel matrix along with a softer coating (such as a metallic layer) will increase the adhesion of the hard particles to the coating.
5. Hard ceramic particle reinforced stainless steel coatings can be used in applications where corrosive resistance is important but the mechanical properties of stainless steels are not sufficient.

Article Information Form

Acknowledgments

We would like to thank Ratetech Advanced Technological Materials Industry and Trade Inc. for providing the production of the coatings examined in this study.

Declaration of Conflict of Interest/Common Interest

The authors declare no conflict of interest or common interest.

Artificial Intelligence Statement

No artificial intelligence tools were used while writing this article.

Authors' Contribution

Conceptualization, O.K.; methodology, O.K.; software, O.K. and S.G.; validation, O.K., S.G.; formal analysis, E.E.; investigation, O.K.; resources, O.K.; data curation, O.K.; writing - original draft preparation, O.K.; writing - review and editing, O.K.; visualization, O.K.; supervision, E.E.; project administration, E.E.;

Copyright Statement

Authors own the copyright of their work published in the journal and their work is published under the CC BY-NC 4.0 license.

References

- [1] V. K. Champagne, O. C. Ozdemir, A. Nardi, *Practical Cold Spray*, Springer, 2021.
- [2] A. Moridi, S. M. Hassani-Gangaraj, M. Guagliano, M. Dao, "Cold spray coating: Review of material systems and future perspectives," *Surface Engineering*, vol. 36, no. 6, pp. 369–395, 2014.
- [3] E. Tekin, S. Uyum, B. Karahan, K. C. Tekin, U. Malayoğlu, "Soğuk püskürtme teknolojisi ve uygulamaları," *Mühendis ve Makina*, vol. 62, no. 702, pp. 106–150, 2021.
- [4] H. Assadi, H. Kreye, F. Gärtner, T.J.A.M. Klassen, "Cold spraying—A materials perspective," *Acta Materialia*, vol. 116, pp. 382-407, 2016.
- [5] Y. Wei, W. Zhang, J. Zhang, Y. Wang, X. Chu, S. Qi, et al., "Preparation of highly dense Ti-based coatings with enhanced corrosion protection performance via cold spray," *Surface and Coatings Technology*, vol. 473, p. 130002, 2023.
- [6] M. R. Rokni, S. R. Nutt, C. A. Widener, "Review of Relationship between Particle Deformation, Coating Microstructure, and Properties in High-Pressure Cold Spray," *Journal of Thermal Spray Technology*, vol. 26, pp. 1308–1355, 2017.
- [7] M. Ashokkumar, D. Thirumalaikumarasamy, P. Thirumal, R. Barathiraja, "Influences of Mechanical, Corrosion, erosion and tribological performance of cold sprayed Coatings A review," *Materials Today: Proceedings*, vol. 46, pp. 7581-7587, 2021.
- [8] K. Kılıçay, "A practical approach to fabrication of nano-Al₂O₃ reinforced MMC coatings by cold spray: Characterization of nanomechanical and tribological performance," *Materials Today Communications*, vol. 39, p. 109257, 2024.
- [9] A. Sai Jagadeeswara, S. Kumara, B. Venkataramanb, P. Suresh Babua, A. Jyothirmayi, "Effect of thermal energy on the deposition behaviour, wear and corrosion resistance of cold sprayed Ni-WC cermet coatings," *Surface and Coatings Technology*, vol. 399, p. 126138, 2020.
- [10] D. I. Adebisi, A. P. I. Popoola, I. Botef, "Low pressure cold spray coating of Ti-6Al-4V with SiC-based cermet," *Materials Letters*, vol. 175, pp. 63-67, 2016.
- [11] G. Santacruz, Vicente Albaladejo, A. Silvello, R. F. Vaz, C. P'erez Bergmann, I. G. Cano, "The critical role of liquid surface tension in determining cavitation erosion and dry wear performance of WC-17Co coatings produced by cold spray technology," *Tribology International*, vol. 208, p. 110609, 2025.
- [12] J. Selvaraj, K. Balakrishnan, K. Raja, I. Charit, V. "Subramanian, A comparative review on cold sprayed cermet coatings and their applications in high temperature corrosion, oxidation and wear resistance," *Results in Surfaces and Interfaces*, vol. 20, p. 100589, 2025.
- [13] Z. Eyvazi, A. Abdollah-zadeh, R.A. Seraj, A. Azarniya, "Effect of SiC content on the microstructure and wear behavior of cold-sprayed Al-SiC coatings deposited on AZ31 alloy substrate," *Surface and Coatings Technology*, vol. 489, p. 131170, 2024.